ACS APPLIED MATERIALS & INTERFACES

Research Article

www.acsami.org

Environmentally Assisted Cracking in Silicon Nitride Barrier Films on Poly(ethylene terephthalate) Substrates

Kyungjin Kim, Hao Luo, Ankit K. Singh, Ting Zhu, Samuel Graham,* and Olivier N. Pierron*

George W. Woodruff School of Mechanical Engineering, Georgia Institute of Technology, Atlanta, Georgia 30332, United States

Supporting Information

ABSTRACT: A singular critical onset strain value has been used to characterize the strain limits of barrier films used in flexible electronics. However, such metrics do not account for time-dependent or environmentally assisted cracking, which can be critical in determining the overall reliability of these thin-film coatings. In this work, the time-dependent channel crack growth behavior of silicon nitride barrier films on poly(ethylene terephthalate) (PET) substrates is investigated in dry and humid environments by tensile tests with in situ optical microscopy and numerical models. The results reveal the occurrence of environmentally assisted crack growth at strains well below the critical onset crack strain and in the absence of polymer-relaxation-assisted, time-dependent crack growth. The crack growth rates in laboratory air are about 1 order of magnitude larger than those tested in dry environments (dry air or dry nitrogen). In laboratory air, crack growth rates increase from ~200 nm/s to 60 μm/s for applied stress intensity factors, K, ranging from 1.0 to 1.4 MPa·m$^{1/2}$, below the measured fracture toughness K_c of 1.8 MPa·m$^{1/2}$. The crack growth rates in dry environments were also strongly dependent on the prior storage of the specimens, with larger rates for specimens exposed to laboratory air (and therefore moisture) prior to testing compared to specimens stored in a dry environment. This behavior is attributed to moisture-assisted cracking, with a measured power law exponent of ~22 in laboratory air. This study also reveals that much larger densities of channel cracks develop in the humid environment, suggesting an easier initiation of channel cracks in the presence of water vapor. The results obtained in this work are critical to address the time-dependent and environmental reliability issues of thin brittle barriers on PET substrates for flexible electronics applications.

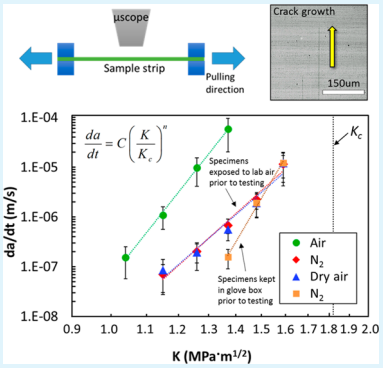

KEYWORDS: *PECVD, silicon nitride, PET, time-dependent cracking, polymer relaxation*

1. INTRODUCTION

Barrier layers that contain ultrathin inorganic hard coatings on poly(ethylene terephthalate) (PET) substrates have become indispensable in the flexible electronics industry for maintaining reliable operation of devices, with the most notable demand from organic light-emitting diodes for flexible displays and thin-film solar cells. For these applications, various barrier film architectures (multilayer stacks) and processing methods (PECVD, ALD, etc.) have been developed to create ultrabarrier films with an effective water vapor transmission rate (WVTR) less than 10^{-4} g·m^{-2}·day^{-1}. Of these methods, multilayer amorphous silicon nitride (SiN_x) thin films fabricated by plasma-enhanced chemical vapor deposition (PECVD) have recently found success in the development of flexible ultrabarrier coatings with WVTR on the order of 10^{-6} g·m^{-2}·day^{-1} and have also been demonstrated on flexible displays.[1−7] SiN_x films can be deposited at low temperatures (~100 °C) and high deposition rates (60 nm/min) while exhibiting great barrier film qualities, such as low porosity and excellent transparency.[8−11] Moreover, residual stresses can be controlled through the PECVD deposition conditions of substrate temperature, plasma power, chamber gas pressure, and chemical composition (i.e., ratio of silicon to nitride in this case).[12,13] This allows the SiN_x films to have compressive residual stresses, which help prevent pre-existing microcracks from growing without applied external loads.[14]

Flexible electronics are by design meant to be subjected to applied strains. It is therefore of paramount importance to study the mechanical reliability of the inherently brittle barrier coatings, including channel cracking of the coating and its debonding from the PET substrate. Most of the related reliability studies have so far focused on determining the critical onset strains to failure and density of cracks.[15−23] For example, George and co-workers[15−17] specifically studied nanoscale atomic and molecular layer deposition (ALD and MLD) layers. Leterrier and co-workers[18−20] also reported that inherent microdefects in inorganic films initiate crack propagation. However, when the application of these barriers to flexible electronics is considered, the strains applied may be much different than the monotonic loading that is found in most of the studies for crack onset strain. This includes the application of fixed strains for curved devices or the application of cyclic strains during flexure, both of which may allow time-dependent behavior to occur. Thus, the question arises as to the

Received: May 29, 2016
Accepted: September 19, 2016
Published: September 19, 2016

DOI: 10.1021/acsami.6b06417
ACS Appl. Mater. Interfaces 2016, 8, 27169−27178

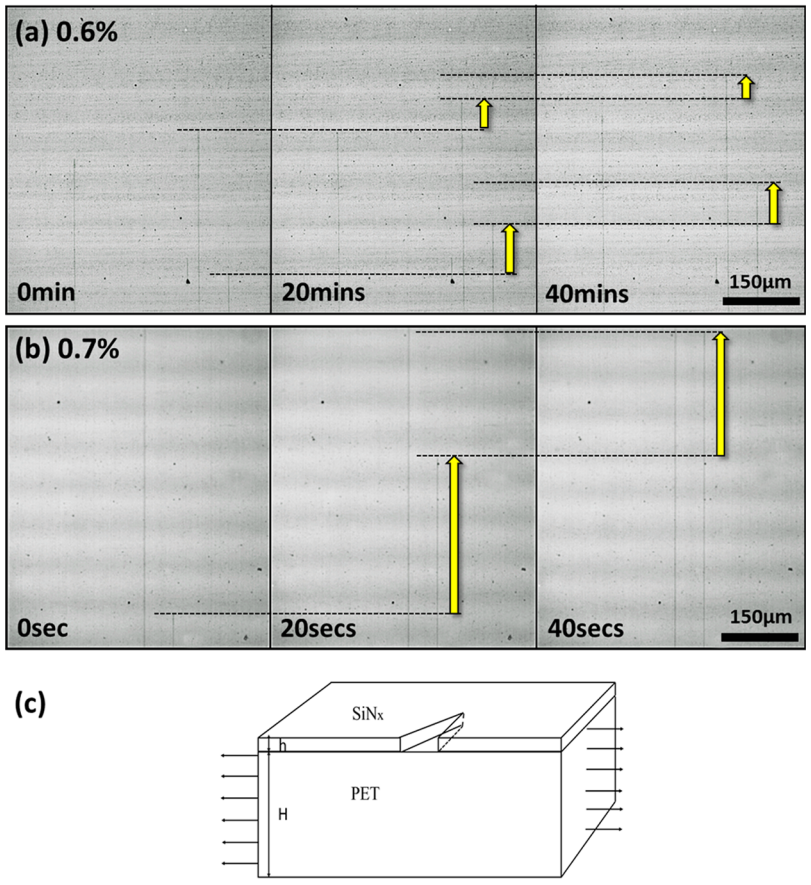

Figure 1. (a, b) Example of time-dependent channel crack growth in 250 nm thick SiN_x in air at strain values of (a) 0.6% and (b) 0.7%. (c) Schematic of crack model. The SiN_x thin film is perfectly bonded to the PET substrate, $h/H = 1/100$.

appropriateness of the use of crack onset strain results for the wide range of loading conditions that may be seen in such coatings in flexible electronic devices, since time-dependent effects are not readily captured by this approach. In fact, Suo and co-workers[24−27] demonstrated that time-dependent cracking of an elastic film made of a material that does *not* undergo any subcritical cracking (i.e., no environmentally assisted cracking or stress corrosion cracking) can occur if a viscous underlayer (i.e., a layer that undergoes creep) is present between the film and an elastic substrate. The physical explanation relies on the following fact: as the underlayer creeps, the stress field relaxes in the crack wake, resulting in a decreased constraint effect of the underlayer on the film and therefore an increased driving force for crack extension (i.e., the stress field around the crack tip intensifies). If, over time, the driving force exceeds a critical value, crack extension occurs: after some amount of cracking, the driving force is reduced due to a larger constraint effect of the underlayer that has not crept yet. The process can repeat itself, and a steady-state crack velocity is attained. Clearly, a similar cracking scenario can occur for thin barriers on PET substrates under tensile strains, depending on the viscous properties of the polymer. Here we studied the time-dependent crack growth properties of SiN_x coatings on poly(ethylene terephthalate) (PET) substrates by considering both polymer creep and subcritical cracking of the SiN_x films, thanks to an integrated experimental and numerical approach.

Many brittle films undergo environmentally assisted subcritical cracking, such as SiO_2 films.[28−31] So far, there are few studies on environmentally assisted cracking of SiN_x films, although environmentally assisted debonding between SiN_x films and Cu has already been demonstrated.[32] Recently, Vellinga et al.[33] observed faster crack propagation in SiN_x barriers on polyethylene naphthalate (PEN) substrates in higher relative humidity surroundings using resistance measurements and in situ microscopy. They argued that this environmental effect was unlikely due to the hygroscopic expansion of the polymer, and instead concluded that SiN_x barriers undergo environmentally assisted cracking. Guan et al.[34] also performed electromechanical two-point bending tests in dynamic and static loading modes to determine the subcritical crack growth exponent n in SiN_x coatings on PEN substrates. Their results suggest that SiN_x thin films behaves differently from bulk Si_3N_4 ceramics that are essentially immune to environmentally assisted cracking.[35,36] However, these studies neither directly measured the crack growth rates as a function of driving force for channel cracking nor considered the aforementioned potential effects of polymer relaxation. It is therefore the goal of this study to characterize and investigate the crack growth behavior of SiN_x films on a PET substrate under different environmental conditions by employing an in situ microscopy technique for measurement of crack growth. Combined with numerical models, this study elucidates the origins of time-dependent crack growth behavior by differentiating the contribution of polymer creep from that of environmentally assisted cracking.

DOI: 10.1021/acsami.6b06417
ACS Appl. Mater. Interfaces 2016, 8, 27169−27178

2. EXPERIMENTAL AND NUMERICAL METHODS

2.1. Deposition and X-ray Photoelectron Spectroscopic Characterization of SiN_x Films on Poly(ethylene terephthalate) Substrate. SiN_x films were deposited on commercial heat-stabilized, 125 μm thick PET (Dupont Teijin Films Melinex ST505). The PET substrate was laser-cut into 50 mm long and 5 mm wide specimens before deposition. SiN_x was then deposited on the PET substrate by use of a Unaxis PECVD system with radio frequency (rf) parallel plate configuration at a temperature of 110 °C, pressure of 1 Torr, and 20 W rf plasma. Silane (SiH_4) and ammonia (NH_3) gases were used as the process gases with flow rates of 12 and 14 sccm, respectively, while 200 sccm of He was used as the carrier gases. The deposition rate was about 10 nm/min, and the film thickness was confirmed by ellipsometry (Wollam M2000 ellipsometer) measurements of a PECVD film deposited on a surrogate Si sample. SiN_x films with thicknesses ranging from 15 to 250 nm were deposited to study the thickness effect on fracture behavior. The time-dependent crack growth study was carried out with 250 nm thick SiN_x films.

Chemical characterization of SiN_x films was conducted with X-ray photoelectron spectroscopy (XPS) on a Thermo Scientific K-Alpha X-ray photoelectron spectrometer system with a monochromatic Al Kα X-ray source ($h\nu$ = 1486.6 eV). The top surface of SiN_x deposited by the PECVD process was etched for 55 s by Ar^+ ion sputtering so as to remove oxidized and contaminated portions on exposure to atmosphere.

2.2. In Situ Optical Microscopy Tensile Tests. A microtensile testing stage (Linkam Scientific Instruments, TST350) was used for all tensile tests, with a load resolution of 0.01 N and displacement resolution of 10 μm. In situ microscopy was used to observe the onset of cracking and/or time-dependent crack propagation during the tests. The observations were made with either a confocal microscope (Olympus LEXT, OLS4100) or an optical microscope (Edmund Optics, 1312 M 59-365). Tests were performed in laboratory air as well as controlled environments. To perform the experiments in inert environments, the tensile stage was sealed and dry air (Airgas, AIUZ300) or nitrogen (Airgas, NI UHP300) was flowing through the stage during the test. Both gases have negligible moisture content (i.e., 2 ppm). For testing in laboratory air, the lid was removed from the Linkam stage and the sample was exposed to the laboratory environment, with an approximate relative humidity content of 30%.

Two different types of test were performed. The first one consisted of measuring the critical onset strain, ε_c, at which the first propagating crack was observed. For these tests, the observation area was kept constant (258 × 258 μm). The values of ε_c were obtained as a function of applied strain rates (0.00025, 0.00125, 0.0025, 0.0125, 0.025, and 0.125%/s) and environment (laboratory vs dry air). These experiments established the occurrence of environmentally assisted and time-dependent cracking. These effects were further characterized by measuring the crack growth rates during relaxation tests in laboratory air and inert environments. The specimens were strained up to a value below ε_c, at which point the displacement was kept constant, and the crack growth behavior was observed by in situ microscopy (see examples in Figure 1a,b). Specifically, the crack growth rates were calculated by averaging the measured rates of the growing cracks (typically 20−30 cracks) tracked through the entire observation area (region with a radius of 13.6 mm). The number of cracks within a fixed area was also calculated (644 × 643 μm). In a few instances, movies of the propagating cracks were taken at a rate of 30 frames/s. Depending upon the speed of crack propagation, the frames were extracted from the video at regular intervals by use of Matlab. The pixel position corresponding to the crack tip was determined, from which the crack length could be determined. The increase in crack length was then plotted against time to determine the overall crack growth behavior and speed.

2.3. Driving Force for Crack Propagation. The mechanics framework for thin-film crack propagation was developed in the 1990s for microelectronics applications.[14,37,38] Cracking in integrated circuits is mainly driven by residual stresses that are often present in the films,[39] while for flexible electronics applications, a mechanical load is also applied. A key concept associated with thin-film channel cracking on substrates is that the driving force (once the crack is long enough with respect to the film thickness) is independent of the crack length (unlike the driving force for freestanding films). This is due to the substrate constraint effect on the relaxed elastic energy in a volume of material around the crack. Instead, the driving force becomes a function of film thickness, its amplitude being governed by the effective constraint provided by the substrate. As a result, the driving force is a strong function of the elastic mismatch between film and substrate, with larger driving forces (less constraint) for compliant substrates/stiff films arrangements, and is given by[38]

$$G_{ss} = \frac{Z\sigma^2 h_f}{E_f^*} = \frac{Z(\sigma_{appl} + \sigma_{res})^2 h_f}{E_f^*} = ZE_f^*(\varepsilon_{appl} + \varepsilon_{res})^2 h_f \quad (1)$$

where σ, σ_{appl}, and σ_{res} are the total, applied, and residual stress in the film, respectively; ε_{appl} and ε_{res} are the applied and residual strains in the film; E_f^* and h_f are the plane strain elastic modulus and thickness of the film; and Z is the dimensionless energy release rate, which depends on the elastic mismatch α between film and substrate:[14]

$$\alpha = \frac{E_f^* - E_s^*}{E_f^* + E_s^*} \quad (2)$$

where E_s^* is the plane strain substrate elastic modulus. Numerical models can provide the value for Z as a function of α.[14,40,41] The energy release rate G_{ss} is related to the stress intensity factor K of the crack by eq 3:[42]

$$K = \sqrt{G_{ss}E_f^*} \quad (3)$$

Equation 1 assumes linear elastic behavior of both film and substrate[38] and dictates the driving force for channel cracking of an isolated crack (whose front width corresponds exactly to the film thickness) on a semi-infinite substrate.[38] The equation can be modified in the case of multiple cracks,[41] thinner substrates,[40,41] delamination, or if the crack tip lies on either side of the interface.[38,43,44] It can also be modified in the case of plastic deformation of the substrate and/or film.[45,46] Local yielding in the substrate results in an increase in driving force. By assuming a constant yield strength at the film−substrate interface, Hu and Evans[46] used a shear lag model to estimate the plastic yielding effect on G_{ss} as

$$G_{ss} = \left(Z + \frac{\sigma}{\sqrt{3}\,\sigma_0}\right) E_f^*(\varepsilon + \varepsilon_{res})^2 h_f \quad (4)$$

where σ is the stress in the coating [$\sigma = E_f(\varepsilon_{appl} + \varepsilon_{res})$] and σ_0 is the yield stress of the substrate.

2.4. Mechanical Characterization of SiN_x Coatings and Poly(ethylene terephthalate) Substrate. As explained in section 2.3, quantification of the driving force G_{ss} for channel crack propagation requires knowledge of several mechanical properties of the film and substrate (see eqs 1 and 4) as well as knowledge of the crack configuration. The SiN_x films can be accurately modeled as a linear elastic material, for which only E_f and ν_f are required. Nanoindentation (Hysitron triboindenter) was used to measure E_f. A 1 μm thick SiN_x coating deposited on a surrogate Si substrate was indented to a depth of 100−300 nm, and a value of E_f = 123 ± 5.81 GPa was obtained. A value of ν_f = 0.253, previously reported for PECVD SiN_x films,[47] was used. The microtensile stage was used to obtain uniaxial tensile properties of the PET substrate (50 mm long, 5 mm wide specimens) along with stress relaxation behavior.

An in situ optical microscopy test was performed to estimate the residual strain, ε_{res}, in the 250 nm thick SiN_x films. In the case of residual compressive strains (as for the SiN_x films), this quantity can be approximated by first straining (in our case up to 0.8%) a specimen so as to form several cracks and then reporting the applied strain upon unloading at which the cracks become close and therefore cannot be observed anymore (see Figure S1). Using this technique, we obtained ε_{res} = −0.15% (±0.02%), corresponding to a compressive residual stress of 185 (±25) MPa for the 250 nm thick SiN_x coatings.

DOI: 10.1021/acsami.6b06417
ACS Appl. Mater. Interfaces 2016, 8, 27169−27178

The crack configuration was obtained from scanning electron microscopic (SEM) images (Hitachi SU8230) of a few cross sections, by use of a focused ion beam (FIB), at the locations of channel cracks. A 10 nm thick layer of Au/Pd was first sputtered on top of the SiN_x coatings to reduce charging effects. Then a 10 μm deep, 30 by 30 μm^2 trench was etched around a channel crack.

2.5. Numerical Model. We evaluated the energy release rate for a long channel crack in a SiN_x thin film on a PET substrate by using the finite element package ABAQUS.[48] To this end, we adopted a linear elastic model for SiN_x and an elastic-viscoplastic model for PET. The latter allows us to account for both plastic yielding and viscous relaxation that may occur in a highly deformed region of PET near the crack. In the one-dimensional (1D) representation of a three-dimensional (3D) elastic–viscoplastic model, the total strain rate $\dot{\varepsilon}$ is given by

$$\dot{\varepsilon} = \dot{\varepsilon}_e + \dot{\varepsilon}_p \tag{5}$$

Here the elastic strain rate $\dot{\varepsilon}$ is linearly proportional to the stress rate $\dot{\sigma}$ according to $\dot{\varepsilon}_e = \dot{\sigma}/E_s$. The plastic strain rate is given by a Cowper–Symonds overstress power law:[48]

$$\dot{\varepsilon}_p = D\left[\frac{\sigma}{\sigma_Y(\varepsilon_p)} - 1\right]^{n'} \tag{6}$$

where D and n' are the material constants and $\sigma_Y(\varepsilon_p)$ is the yield stress that depends on the total yield strain ε_p. Figure 1c shows the schematic of our finite element model for evaluating the steady-state energy release rate G_{ss} of a long channel crack in a SiN_x thin film on a PET substrate. In this model, a 250 nm thick SiN_x film is perfectly bonded with a 25 μm thick PET substrate. The in-plane geometry of the film and substrate is 180 × 180 μm^2. The compressive residual stress in the SiN_x film is taken into account. A 90 μm long wedge crack was created in the middle of the SiN_x thin film, and the wedge angle was sufficiently small so as to minimize its impact on the numerical results. We calculated the stress and strain distributions in the cracked system by imposing a displacement-controlled load on the substrate (corresponding to an applied strain rate of 0.027%/s), and then we evaluated G_{ss} using the J-integral approach.[49] To accurately evaluate G_{ss}, we used a fine mesh around the crack tip in both SiN_x and PET, as shown in Figures S2 and S3.

3. RESULTS AND DISCUSSION

3.1. Optical Properties and Chemical Characterization. The refractive index of SiN_x films was measured to be 1.77 at 632.8 nm by ellipsometry. By use of XPS, oxygen was also found in the bulk of SiN_x film, which could have been incorporated in the structure during the deposition process or by diffusion of oxygen and/or water vapor through the pores upon exposure to the atmosphere. XPS spectra (see Figure S4) reveal that the total atomic percent of Si is 44.56%, of which 95.6% is bonded to N while 4.4% is bonded to H. The atomic percentages of N and O are 53.32% and 3.12%, respectively. The ratio of Si/N (0.81) and refractive index determined for the SiN_x used during the experiment are similar to those in the literature.[50,51] Table 1 shows the overall atomic percentages found in the PECVD SiN_x film along with the NIST reference binding energies used to determine the composition.

Table 1. Chemical Composition and Atomic Percentage Found in PECVD SiN_x

element	at. %	phases	binding energy (eV)	ref
Si	44.56	SiN_x (95.6%), SiH_x (4.4%)	101.56 (SiN_x), 99.65 (SiH_x)	62,63
O	3.12		531.98	64
N	52.32		397.59	65

3.2. Driving Force Evaluation. As mentioned in section 2.3, eq 1 is valid only for the following conditions: the channel crack front width corresponds to the film thickness (i.e., the crack does not penetrate into the PET substrate, nor does it delaminate at the interface), the crack is isolated on a semi-infinite substrate, and both substrate and film exhibit a linear elastic behavior. By use of cross section SEM images, the crack tip was confirmed to sit at the film/substrate interface for a specimen tested at 0.7% for 30 min with no sign of delamination. However, for a specimen tested at 0.7% for 5 days, the crack tip was observed to be several micrometers deep inside the PET substrate from the interface, suggesting cracking of the substrate for these long periods of time. In this study, we focus on the time-dependent crack growth behavior over short periods of times (<30 min), for which the crack tip remains at the interface.

Figure 2a shows the measured uniaxial tensile curve of the PET substrate by use of the microtensile stage. The measured

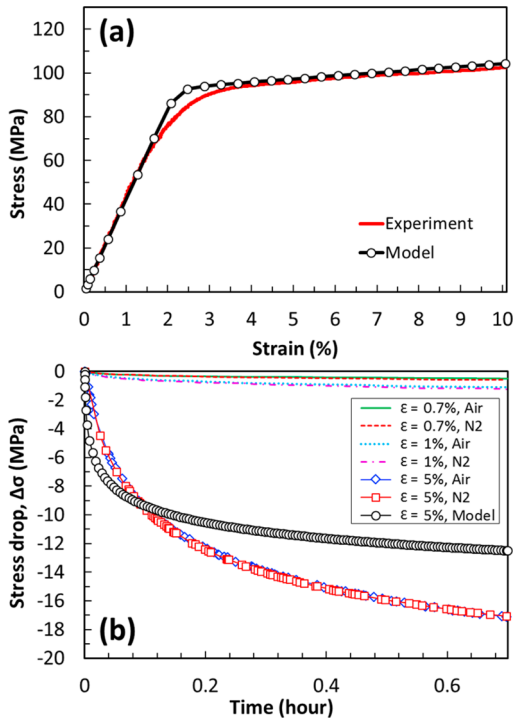

Figure 2. (a) Stress–strain curve and (b) stress relaxation curves of PET substrate.

elastic modulus E_s is 4.07 ± 0.12 GPa, and the 1% offset yield strength of the PET, σ_0, is ~90.6 MPa. A value of ν_s = 0.30 for our PET substrate was used. Table 2 summarizes all the

Table 2. Mechanical Properties of PECVD SiN_x Film and PET Substrate

mechanical properties	PECVD SiN_x film	mechanical properties	PET substrate
E_f	123 ± 5.8 GPa	E_s*	4.47 ± 0.25 GPa
ν_f	0.253	σ_0	90.6 MPa
E_f*	131 ± 6.2 GPa	D	80 h^{-1}
ε_{res}	−0.15% ± 0.02%	n'	20
		σ_y	(50 MPa)(1 + 1.74ε_p)

DOI: 10.1021/acsami.6b06417
ACS Appl. Mater. Interfaces 2016, 8, 27169–27178

relevant mechanical properties for SiN_x films and PET substrate. From the measured E_s^* and E_f^* values, the elastic mismatch is $\alpha = 0.934$, and the corresponding dimensionless energy release rate $Z = 11.8$.[41] Huang et al.[41] studied the effects of substrate finite thickness and channel crack interactions on the driving force G_{ss}. For $\alpha = 0.95$ (a value similar to our bimaterial system), they showed that the semi-infinite substrate case can be approximated for $H/h > 60$, a condition obtained for our 125 μm thick PET/250 nm thick films ($H/h = 500$). G_{ss} is also largely unaffected by neighboring cracks as long as the normalized crack spacing, S/h, is larger than 150, which corresponds in our case to a crack spacing S of 37.5 μm. A significant number of the cracks that we observed meet this criterion. Therefore, we did not consider neighboring crack interaction in the calculation of G_{ss}.

Figure 2a shows that the PET substrate deforms plastically for strains larger than 2.5%. Although all applied strains in this study are less than 1%, the local strains in the PET ahead of the cracks in the SiN_x coating are much larger; hence eq 4 should be used. When eq 4 is compared to eq 1, the driving force G_{ss} is larger by 30−60% due to local yielding of the substrate, as shown in Figure 3 for the range of studied applied strain. We

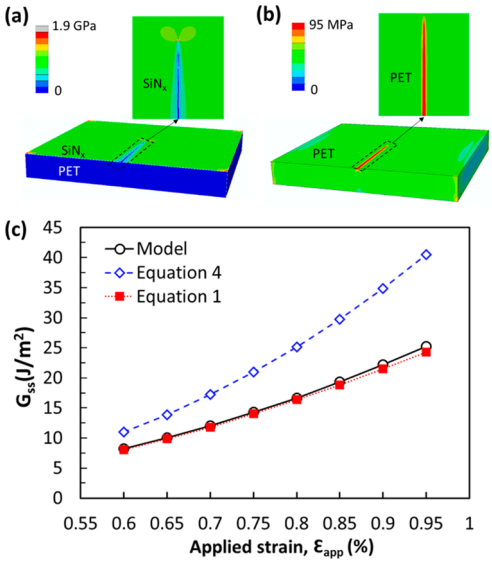

Figure 3. Finite element model and results. (a) von Mises stress contour in SiN_x thin film and PET substrate (lower image) and magnified view of stress concentration around the crack tip in SiN_x thin film (upper image). (b) von Mises stress contour in PET, where high stresses develop beneath the crack wake in PET. (c) Calculated G_{ss} vs ε_{app}, compared to eqs 1 and 4.

used finite element modeling to assess the accuracy of eq 4. First, we determined the viscoplastic parameters of PET by fitting both the experimental tensile stress−strain curve and stress relaxation curves (see Figure 2b, showing six stress relaxation curves of PET for two different environments (air and dry N_2) and three different strain levels (0.7%, 1%, and 5%)]. We obtained $D = 80$/hour, $n' = 20$, and $\sigma_y(\varepsilon_p) = (50\ \text{MPa})(1 + 1.74\varepsilon_p)$; see Table 2. Figure 2 shows that the fitting curves are in close agreement with the experimental results of PET. Figure 3a shows the von Mises stress contour in the system at an applied strain load of 0.95% with a compressive residual strain of $\varepsilon_{res} = -0.15\%$ in the SiN_x thin film (corresponding to 195 MPa residual stress). Stress concentration occurs near the crack tip in SiN_x, in spite of the constraint from PET underneath.[25] Figure 3b shows the von Mises stress contour in the PET at the same load. It is seen that high stresses develop in the PET beneath the crack wake. Under the applied strain of 0.95%, the far-field stress in the PET is only about 40 MPa, while the stress in PET underneath the crack wake reaches 95 MPa, indicating that plastic yielding has occurred in this part of PET. Such local plastic deformation in PET arises due to the opening displacement of the crack face. This in turn allows for a larger crack opening than what an elastic PET model would predict. This result underscores the importance of incorporating plastic yielding in the model. On the basis of the crack-tip field, we obtained the corresponding $G_{ss} = 25.2$ N/m using the J-integral approach in ABAQUS. In comparison, the value obtained for this system by use of eq 4 is $G_{ss} = 40.5 \pm 2.46$ N/m (see Figure 3c). This discrepancy arises from the fact that the shear stress in the PET near the interface is nonuniform (from our finite element results) and hence the simplified shear lag model[46] with a constant interface shear yield strength is not applicable to the present case. In the following results, the modeling curve shown in Figure 3c is deemed more accurate and therefore used to evaluate G_{ss} as a function of the applied strains for the 250 nm thick SiN_x films.

Figure 2b also shows a significant amount of stress relaxation of the PET for strains of 5%, which is likely to occur locally ahead of the crack tips. As explained in the Introduction, the creep of a viscous sublayer induces time-dependent crack growth in the film. Huang et al.[25] studied analytically and numerically the increase in driving force with time for several crack geometries. Their numerical solutions apply only for thin viscous sublayers for which a shear lag model could be used. For thick viscous layers (as is the case with our PET substrate), a 3D viscous flow problem needs to be solved numerically to calculate the driving force, which was done with our numerical model. Specifically, the simulated crack system was held at the applied strain of 0.95% for 0.5 h. Figure 4a−d shows the evolution of stress distribution in PET beneath the crack wake. Figure 4e shows the corresponding peak stress as a function of time, which drops from 95 MPa at time $t = 0$ to 82 MPa at $t = 0.5$ h. However, such viscous stress relaxation in PET has a

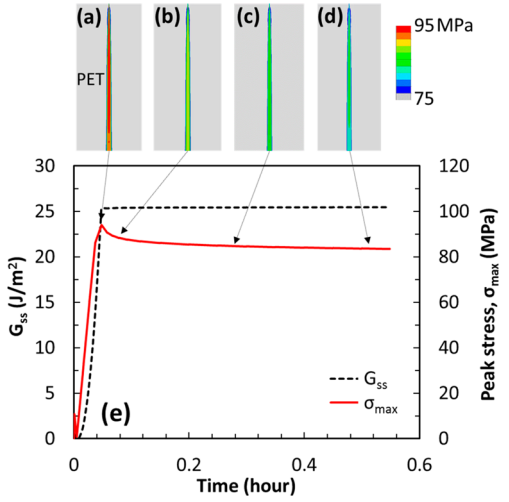

Figure 4. Time evolution of energy release rate and stress beneath the crack wake in PET. (a−d) von Mises stress contour in PET at different times as indicated in panel e, showing the viscous stress relaxation effect. (e) Peak stress in PET and corresponding energy release rate for film cracking as a function of time.

DOI: 10.1021/acsami.6b06417
ACS Appl. Mater. Interfaces 2016, 8, 27169−27178

minor influence on the increase of G_{ss} in the SiN_x thin film; as shown in Figure 4e, G_{ss} increases only slightly, from 25.2 N/m at t = 0 to 25.4 N/m at t = 0.5 h. Therefore, the effect of viscous relaxation on G_{ss} is negligible at low strain loads of less than 1% within the time scale of 0.5 h.

3.3. Fracture Energy Calculation. By use of our numerical model (see Figure 3c), the critical energy release rate (G_c) was calculated to be 25.2 ± 1.26 J/m^2 for the 250 nm thick coatings, corresponding to a fracture toughness (K_{Ic}) value of 1.82 ± 0.03 MPa·m$^{1/2}$ (by use of eq 3). It should be noted that K_{IC} is equivalent to K_c since we are dealing with mode I loading for the samples being tested. These values were obtained from tests performed at a strain rate of 0.05%·s^{-1} to obtain the critical onset strain, ε_c (ε_c = 0.95% ± 0.02% for h_f = 250 nm). This K_{Ic} value is slightly larger than the values (ranging from 1.54 to 1.73 MPa·m$^{1/2}$) measured with microbeams made of PECVD SiN_x.[52] Our measured values constitute an upper limit on the actual K_{Ic}, given that the tests consist of detecting cracking in a small area (258 × 258 μm^2) within a large specimen (50 × 5 mm^2). K_{Ic} values were also calculated for our thinner SiN_x films (see Figure 5), by adapting

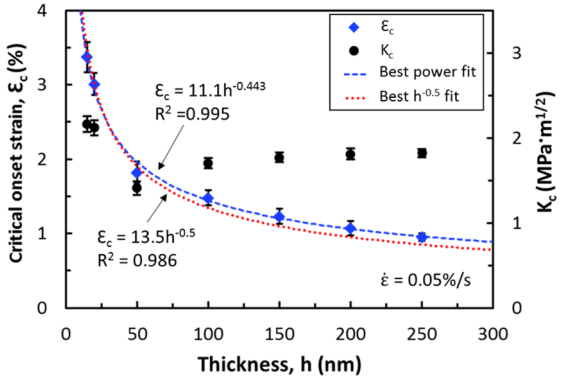

Figure 5. Influence of thickness on ε_c and K_c for SiN_x on PET substrate.

our numerical model to thinner coatings, based on the measured ε_c as a function of coating thickness (also shown in Figure 5). As mentioned above, residual compressive strains were not measured for other thicknesses and were therefore approximated as being equal to the residual strains measured for h_f = 250 nm. Figure 5 shows that K_{Ic} for thicknesses ranging from 50 to 200 nm are fairly similar to the values calculated for h_f = 250 nm, meaning these material properties are thickness-independent (as should be expected for a linear elastic, brittle material).[42] One source of discrepancy for the slightly varying values between different thicknesses may be that the residual stresses vary with thickness. Additionally, it is likely that, as the applied strains (exceeding 3%) are so large for the 15 and 20 nm thick coatings, cracking in the polymer occurs at the crack tip, in which case the current numerical model without consideration of cracking would not be accurate. A power-law fit of the data from Figure 5 gives $\varepsilon_c = 1.11h^{-0.443}$ (R^2 = 0.995), as opposed to the classical $h^{-1/2}$ scaling (see eq 1), which likely results from these considerations [small-scale plasticity of the substrate, thickness-dependent residual strains, and departure from ideal channel crack geometry (i.e., no substrate damage)]. However, a $h^{-1/2}$ power equation can also fit the data fairly well (R^2 = 0.986), especially given the error bars associated with ε_c measurements (see Figure 5). This implies that eq 1 can reasonably predict the thickness dependence, despite the above considerations, as observed experimentally with previous studies on ultrathin coatings.[15] As shown next for the case of the 250 nm thick SiN_x coatings, the safe range of applied strains actually needs to be further decreased due to time-dependent cracking.

3.4. Time-Dependent Crack Growth. Figure 6 shows the measured ε_c as a function of applied strain rate in laboratory

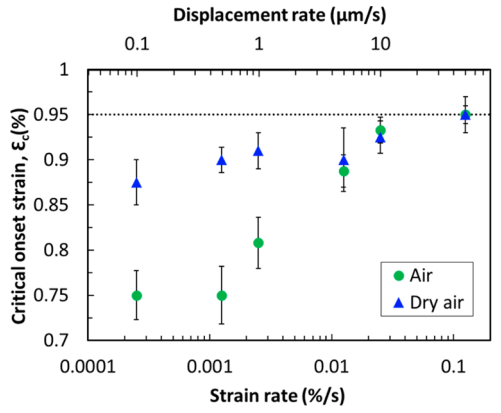

Figure 6. Effect of strain rate on critical onset strain of 250 nm thick SiN_x in air and dry air at room temperature.

(humid) air and dry air environments. The results clearly show that ε_c is a function of both applied strain rate and environmental condition. In humid air, the critical onset strain decreases from 0.95% ± 0.02% to 0.75% ± 0.03% by decreasing the applied strain rate from 10^{-1} to 3 × 10^{-4} %·s^{-1}, while in dry air, the corresponding decrease in critical onset strain was only from 0.95% ± 0.01% to 0.88% ± 0.03%. The lower measured ε_c for lower strain rates suggest time-dependent crack growth (channel cracking) of existing cracks that would be on the order of the time scale for the test observation. As the strain rate is increased above 0.01%·s^{-1}, ε_c becomes independent of the environment. The effect of strain rate on ε_c is consistent with the study by Guan et al.,[34] and the effect of humidity on time-dependent crack growth is consistent with the study by Vellinga et al.[33] Both studies demonstrated environmentally assisted cracking of the SiN_x coatings on PEN polymers. Here, the crack growth rates and behavior were further characterized as a function of applied strains (from 0.6% to 0.85%)/driving forces (see numerical model in Figure 3c for corresponding G_{ss}), in different environments (laboratory air, dry nitrogen, dry air). In our calculations, we ignored the effects of hygroscopic expansion on K. On the basis of a coefficient of hygroscopic expansion of 8 × 10^{-6}/% relative humidity (RH) for our PET, we approximate an increase in applied strain of 0.024% from a dry environment to laboratory air (~30% RH). This results in a small decrease in applied stress in the case of displacement-controlled tests in laboratory air compared to dry environments. The effect on Z (and therefore on the driving force) is deemed negligible (the elastic mismatch, α = 0.934, increases by ~0.2% in laboratory air).

The in situ observation of crack growth confirmed different behavior depending on the humidity content (no difference was observed between dry air and dry nitrogen). First of all, the number of growing cracks was significantly larger in humid air compared to dry nitrogen (see Figure 7b), with more than 10 times more cracks in the humid environment at both 0.6% and

DOI: 10.1021/acsami.6b06417
ACS Appl. Mater. Interfaces 2016, 8, 27169−27178

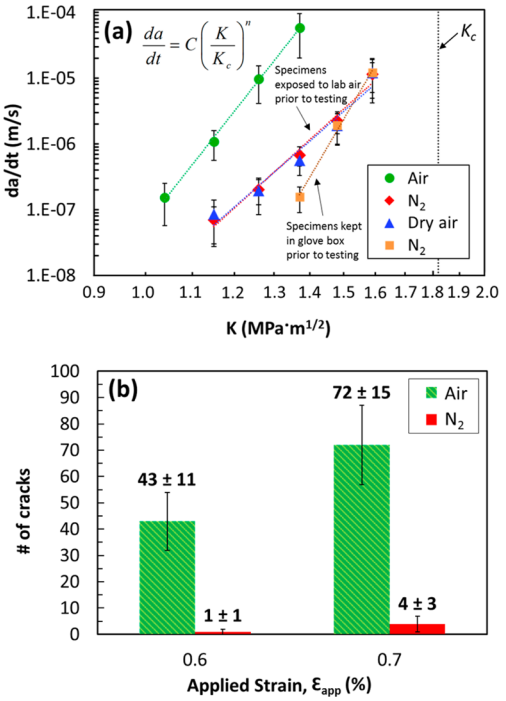

Figure 7. (a) Measured crack growth rates of 250 nm thick SiN_x as a function of stress intensity factor in air (green circles), nitrogen (red diamonds), and dry air (blue triangles). (b) Density of cracks in air and in nitrogen measured 30 min after first observed crack.

0.7% applied strain. The cracks were also observed to grow faster (by ~1 order of magnitude) in the humid environment. As shown in Figure 7a, the average measured crack growth rates were also highly sensitive to the driving force K (i.e., applied strain), thereby explaining the aforementioned strain rate effects on critical onset strain. For example, in humid air, the crack growth rate at ε_{appl} = 0.75% (K = 1.37 MPa·m$^{1/2}$) is ~58.7 ± 38.4 μm·s^{-1}, which would explain the observed decrease in critical onset strain from 0.95% ± 0.02% at an applied strain rate of ~0.1%·s^{-1} (corresponding to a displacement rate of 50 μm·s^{-1}) to 0.75% ± 0.03% at an applied strain rate of ~3 × 10^{-4} %·s^{-1} (corresponding to a displacement rate of 0.1 μm·s^{-1}).

The influence of humidity is further highlighted by considering the effect of specimen storage prior to testing. In our initial testing procedure, specimens tested in dry environments were exposed to laboratory air prior to testing, which may have allowed moisture to absorb at the specimen's surface and diffuse into the SiN_x coating and therefore enable further time-dependent crack growth. Therefore, some specimens were kept in a dry environment (glovebox) prior to testing. Prior to SiN_x deposition, these specimens were also kept in the vacuum deposition chamber at 110 °C for 1 h in order to minimize the moisture content in PET. As shown in Figure 7a, crack growth rates are further decreased for these specimens, stored in dry conditions and tested in dry N_2, compared to the specimens tested in dry environments but exposed to laboratory air prior to testing. A power law equation was used to fit the data:

$$\frac{da}{dt} = C\left(\frac{K}{K_c}\right)^n \quad (7)$$

with coefficients C and n listed in Table 3 as a function of environment and specimen storage.

Table 3. Coefficients n and C as a Function of Environment and Specimen Storage Conditions

specimen storage	environment	n	C (m/s)
exposed to air	air	21.8	2.78 × 10^{-2}
exposed to air	N_2	15.5	6.91 × 10^{-5}
exposed to air	dry air	15.0	5.65 × 10^{-5}
kept in dry conditions	N_2	29.3	6.89 × 10^{-4}

These average rates were calculated only from growing cracks that were not interacting with particles present on the PET substrate before deposition. Figure 8 shows the measured

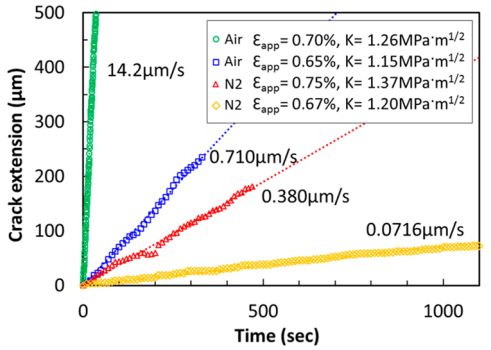

Figure 8. Crack extension as a function of time.

length extension over time for four isolated cracks (two different strain levels in dry N_2 and laboratory air) that did not have particles in their path. This figure shows smooth crack growth at constant rates that are consistent with that shown in Figure 7a. However, the in situ microscopic observations revealed drastically different channel crack growth behavior in films where large densities of contaminants/particles were present (occurrence of these particles depends on handling of the PET substrate prior to deposition). In dry N_2, at applied strains of 0.85% (corresponding to stable crack growth of 11.6 ± 5.50 μm/s in the absence of particles), it was observed that cracks grew from particles at rates too large to be measured, after an incubation period. The cracks grew at these large rates until they reached other particles and were arrested. After another incubation period, the cracks started again propagating from the particles at rates too large to be measured, until they again reached more particles, and the process repeated itself. The incubation period was measured to increase with decreasing applied strains (from ~250 ± 150 s at 0.9% to 900 ± 650 s at 0.75%). Importantly, this unstable crack growth behavior in the presence of particles was not observed when the tests were performed in laboratory air.

As mentioned above, time-dependent crack growth due to PET creep is unlikely to occur due to the minor effect of PET stress relaxation on the increase of G_{ss} within a time scale of 0.5 h. Hence, we conclude that environmentally assisted cracking of SiN_x governs the observed behavior in humid air. Given that the crack growth behavior is similar between dry nitrogen and dry air, and given the importance of specimen storage that likely impacts the moisture content in the specimen or at the specimen's surface, our results indicate that water molecules are the chemically active species in the crack growth process (and not oxygen). It is possible that traces of water in the dry environments (~2 ppm) and/or adsorbed water at the surface of the PET polymer before the coating deposition could lead to environmentally assisted cracking to some degree in these

DOI: 10.1021/acsami.6b06417
ACS Appl. Mater. Interfaces 2016, 8, 27169−27178

environments. This would explain the increased rates observed in dry N_2 for the specimens stored in laboratory air prior to testing. Region I of the $da/dt-K$ curve for soda lime silica is a strong function of water concentration.[53,54] The environmentally assisted cracking of our SiN_x coatings is therefore reminiscent of the stress corrosion cracking in glass, which relies on a stress-enhanced chemical reaction between water and glass at the highly stressed crack tip.[55,56] At a crack tip in SiN_x coatings, chemical attack from invading water molecules could enhance the rate of Si−N bond breaking and accordingly the rate of crack growth, owing to the stress-assisted hydrolysis reaction similar to the surface dissolution of Si_3N_4: $Si_3N_4 + 6H_2O \rightarrow 3SiO_2 + 4NH_3$.[57]

The results also strongly suggest that the presence of water vapor affects the initiation of channel cracks. While similar crack growth rates (~100 nm·s^{-1}) are measured in humid air at an applied strain of 0.6% (K = 1.0 MPa·m$^{1/2}$) and in dry N_2 at 0.7% (K = 1.3 MPa·m$^{1/2}$) (see Figure 7a), the average measured number of cracks is 43 in air versus four in N_2 (see Figure 7b). A possible explanation is that the environment accelerates the subcritical growth of surface flaws into channel cracks. Equations 1 and 6 apply only to the growth of long channel cracks, not their initiation. An underlying assumption often made to use these equations is that the long channel cracks are initially present in the coatings. If this were the case, there should not be 10 times more channel cracks in air than in dry N_2 for similar channel crack velocities. Instead, we hypothesize that smaller defects, such as surface flaws, are present. These surface flaws are initially surrounded by the hard SiN_x (for example, assume a semielliptical surface flaw with a depth less than the coating thickness). When exposed to the environment, these surface flaws may grow in a self-similar fashion thanks to environmentally assisted cracking until they reach the interface and transition to a channel crack.

The issue of nucleating versus propagating a channel crack may also explain the observed environment-dependent crack growth behavior in the presence of particles (described above). In dry N_2, much faster crack propagation starting from particles occurs after an incubation period that increases with decreasing applied strains, a behavior that is not observed in humid air (only stable crack propagation at measurable crack growth rates was observed in this environment for similar applied strains). A possible explanation is that, as a channel crack is arrested at a particle, polymer relaxation occurs (at a larger rate due to the particle's stress concentration effect), leading to an increasing stress field. Since the channel crack is not present on the other side of the particle (from where the channel crack arrested), it needs to be nucleated. It is possible that the stress required to nucleate the channel crack is, under these conditions, larger than the stress required to propagate the channel crack; hence, once the channel crack is nucleated, the driving force G_{ss} is large enough to provide fast crack propagation. This explanation would be consistent with longer incubation periods that were measured for lower applied strains (as it would take more time to intensify the stress field ahead of the particle). In humid air, fast crack propagation from particles was not observed (meaning G_{ss} did not significantly increase), which could be the result of fast, environmentally assisted nucleation of channel cracks, as explained above. This reasoning holds only if the stress concentration effect of the particle is large enough to allow significant polymer relaxation effects. This singular effect of particles on time-dependent cracking in SiN_x coatings deserves further investigation and highlights the challenges of accurately predicting cracking in coatings that contain particles.

As a concluding remark, we note that the time-dependent results described in this paper need to be restricted to short times (~30 min) after channel cracking is first observed. As mentioned in section 3.2, our FIB cross sections revealed cracking of the polymer at the location of channel cracks. Further study is therefore required to capture the evolution of driving force with time for channel crack propagation in the case of evolving substrate damage and to correlate it with the observed crack growth behavior under much longer time exposures (~days). This knowledge is also crucial to assess the long-term reliability of flexible electronics requiring thin film barriers.[58−60]

4. CONCLUSIONS

In summary, we have found the use of a critical strain ε_c at high strain rates to be insufficient to define the safe operating envelope against channel cracking for SiN_x barrier films on PET substrates, due to time-dependent crack growth. Specifically, it was shown that the channel crack growth in SiN_x barrier films can occur at strain levels 35% below the apparent ε_c due to environmentally assisted crack growth. The $da/dt-K$ curves were obtained for 250 nm thick films on 125 μm thick PET in humid and dry environments and as a function of storage conditions prior to testing. Numerical models were instrumental in calculating the driving force K and in revealing that polymer relaxation during the displacement-controlled cracking tests has only a minor effect on time-dependent crack growth. The crack growth rates were higher by a factor of 10 in humid air versus dry nitrogen. In dry environments, the rates were also strongly affected by the specimen storage condition, with faster crack growth for specimens exposed to laboratory air prior to testing. This behavior likely results from moisture-assisted cracking, with a measured power law exponent of ~22 in laboratory air and ~29 in dry N_2 for specimens stored in a dry environment prior to testing. A higher channel crack density was also measured in humid air, highlighting the role of humidity on the nucleation of channel cracks. The analysis presented in this work is valuable because environmentally dependent crack growth behavior has been appropriately characterized for the first time in barrier films on flexible substrates to better define the reliability of hermetic coatings for flexible devices. We expect that this approach of testing can be widely used for other thin barrier films since the state of the art technology adopted allows for in situ visualizations down to 15 nm in thickness.[61]

■ ASSOCIATED CONTENT

Supporting Information

The Supporting Information is available free of charge on the ACS Publications website at DOI: 10.1021/acsami.6b06417.

Four figures showing residual strain measurement and XPS data of sample, as well as meshing scheme and contour selection for J integral calculation (PDF)

■ AUTHOR INFORMATION

Corresponding Authors

*E-mail sgraham@gatech.edu.
*E-mail olivier.pierron@me.gatech.edu.

Notes

The authors declare no competing financial interest.

DOI: 10.1021/acsami.6b06417
ACS Appl. Mater. Interfaces 2016, 8, 27169−27178

■ ACKNOWLEDGMENTS

We thank Dr. Ehsan Hosseinian for his assistance with the FIB cross-sectioning. T.Z., S.G., and O.N.P. gratefully acknowledge support from NSF CMMI through Award 1400077.

■ REFERENCES

(1) Li, F. M.; Unnikrishnan, S.; van de Weijer, P.; van Assche, F.; Shen, J.; Ellis, T.; Manders, W.; Akkerman, H.; Bouten, P.; van Mol, T. 18.3: Flexible Barrier Technology for Enabling Rollable AMOLED Displays and Upscaling Flexible OLED Lighting. *Dig. Tech. Pap. - Soc. Inf. Disp. Int. Symp.* **2013**, *44* (1), 199−202.

(2) Bulusu, A.; Singh, A.; Wang, C. Y.; Dindar, A.; Fuentes-Hernandez, C.; Kim, H.; Cullen, D.; Kippelen, B.; Graham, S. Engineering the Mechanical Properties of Ultrabarrier Films Grown by Atomic Layer Deposition for the Encapsulation of Printed Electronics. *J. Appl. Phys.* **2015**, *118* (8), No. 085501.

(3) Andringa, A.-M.; Perrotta, A.; De Peuter, K.; Knoops, H. C. M.; Kessels, W. M. M.; Creatore, M. Low-Temperature Plasma-Assisted Atomic Layer Deposition of Silicon Nitride Moisture Permeation Barrier Layers. *ACS Appl. Mater. Interfaces* **2015**, *7* (40), 22525−22532.

(4) Majee, S.; Geffroy, B.; Bonnassieux, Y.; Bouree, J.-E. Interface Effects on the Moisture Barrier Properties of SiNx/PMMA/SiNx Hybrid Structure. *Surf. Coat. Technol.* **2014**, *254*, 429−432.

(5) Rochat, G.; Fayet, P. Characterization of Mechanical Properties of Ultra-thin Oxide Coatings on Polymers by Uniaxial Fragmentation Tests. *J. Adhes. Sci. Technol.* **2012**, *26* (20−21), 2381−2392.

(6) van Assche, F. J. H.; Unnikrishnan, S.; Michels, J. J.; van Mol, A. M. B.; van de Weijer, P.; van de Sanden, M. C. M.; Creatore, M. On the Intrinsic Moisture Permeation Rate of Remote Microwave Plasma-deposited Silicon Nitride Layers. *Thin Solid Films* **2014**, *558*, 54−61.

(7) Zhang, S.; Xue, W.; Yu, Z. Moisture Barrier Evaluation of SiOx/SiNx Stacks on Polyimide Substrates Using Electrical Calcium Test. *Thin Solid Films* **2015**, *580*, 101−105.

(8) Wuu, D.; Lo, W.; Chiang, C.; Lin, H.; Chang, L.; Horng, R.; Huang, C.; Gao, Y. Water and Oxygen Permeation of Silicon Nitride Films Prepared by Plasma-enhanced Chemical Vapor Deposition. *Surf. Coat. Technol.* **2005**, *198* (1), 114−117.

(9) Keuning, W.; Van de Weijer, P.; Lifka, H.; Kessels, W.; Creatore, M. Cathode Encapsulation of Organic Light Emitting Diodes by Atomic Layer Deposited Al2O3 Films and Al2O3/a-SiNx: H stacks. *J. Vac. Sci. Technol., A* **2012**, *30* (1), 01A131.

(10) van Assche, F. J.; Unnikrishnan, S.; Michels, J. J.; van Mol, A. M.; van de Weijer, P.; van de Sanden, M. C.; Creatore, M. On the Intrinsic Moisture Permeation Rate of Remote Microwave Plasma-Deposited Silicon Nitride Layers. *Thin Solid Films* **2014**, *558*, 54−61.

(11) Martyniuk, M. P.; Antoszewski, J.; Musca, C. A.; Dell, J. M.; Faraone, L. In Determination of Residual Stress in Low-temperature PECVD Silicon Nitride Thin Films, Microelectronics, MEMS, and Nanotechnology. *Proc. SPIE* **2003**, 451−462.

(12) Huang, H.; Winchester, K. J.; Suvorova, A.; Lawn, B. R.; Liu, Y.; Hu, X. Z.; Dell, J. M.; Faraone, L. Effect of Deposition Conditions on Mechanical Properties of Low-temperature PECVD Silicon Nitride Films. *Mater. Sci. Eng., A* **2006**, *435−436*, 453−459.

(13) Huang, H.; Winchester, K.; Liu, Y.; Hu, X. Z.; Musca, C. A.; Dell, J. M.; Faraone, L. Determination of Mechanical Properties of PECVD Silicon Nitride Thin Films for Tunable MEMS Fabry−Pérot Optical Filters. *J. Micromech. Microeng.* **2005**, *15* (3), 608−614.

(14) Beuth, J. L. J. Cracking of Thin Bonded Films in Residual Tension. *Int. J. Solids Struct.* **1992**, *29* (13), 1657−1675.

(15) Jen, S.-H.; Bertrand, J. A.; George, S. M. Critical Tensile and Compressive Strains for Cracking of Al2O3 Films Grown by Atomic Layer Deposition. *J. Appl. Phys.* **2011**, *109* (8), 084305.

(16) Jen, S.-H.; Lee, B. H.; George, S. M.; McLean, R. S.; Carcia, P. F. Critical Tensile Strain and Water Vapor Transmission Rate for Nanolaminate Films Grown Using Al_2O_3 Atomic Layer Deposition and Alucone Molecular Layer Deposition. *Appl. Phys. Lett.* **2012**, *101* (23), 234103.

(17) Miller, D. C.; Foster, R. R.; Zhang, Y.; Jen, S.-H.; Bertrand, J. A.; Lu, Z.; Seghete, D.; O'Patchen, J. L.; Yang, R.; Lee, Y.-C.; George, S. M.; Dunn, M. L. The Mechanical Robustness of Atomic-layer- and molecular-layer-deposited Coatings on Polymer Substrate. *J. Appl. Phys.* **2009**, *105* (9), 093527.

(18) Leterrier, Y. Durability of Nanosized Oxygen-barrier Coatings on Polymers. *Prog. Mater. Sci.* **2003**, *48* (1), 1−55.

(19) Andersons, J.; Modniks, J.; Leterrier, Y.; Tornare, G.; Dumont, P.; Månson, J. A. E. Evaluation of Toughness by Finite Fracture Mechanics from Crack Onset Strain of Brittle Coatings on Polymers. *Theor. Appl. Fract. Mech.* **2008**, *49* (2), 151−157.

(20) Leterrier, Y.; Andersons, J.; Pitton, Y.; Månson, J. A. Adhesion of Silicon Oxide Layers on Poly (Ethylene Terephthalate). II: Effect of Coating Thickness on Adhesive and Cohesive Strengths. *J. Polym. Sci., Part B: Polym. Phys.* **1997**, *35* (9), 1463−1472.

(21) Lewis, J. Material Challenge for Flexible Organic Devices. *Mater. Today* **2006**, *9* (4), 38−45.

(22) Lewis, J.; Grego, S.; Vick, E.; Chalamala, B.; Temple, D. Mechanical Performance of Thin Films in Flexible Displays. *MRS Proc.* **2004**, *814*, I8.5.

(23) Behrendt, A.; Meyer, J.; van de Weijer, P.; Gahlmann, T.; Heiderhoff, R.; Riedl, T. Stress Management in Thin-Film Gas-Permeation Barriers. *ACS Appl. Mater. Interfaces* **2016**, *8* (6), 4056−4061.

(24) Allameh, S. M.; Suo, Z. G.; Soboyejo, W. Creep of Al Underlayer Determined by Channel Cracking of Topical Si(3)N(4) film. *Mater. Manuf. Processes* **2007**, *22* (2), 170−174.

(25) Huang, R.; Prevost, J. H.; Suo, Z. Loss of Constraint on Fracture in Thin Film Structures due to Creep. *Acta Mater.* **2002**, *50* (16), 4137−4148.

(26) Liang, J.; Huang, R.; Prevost, J. H.; Suo, Z. Thin Film Cracking Modulated by Underlayer Creep. *Exp. Mech.* **2003**, *43* (3), 269−279.

(27) Liang, J.; Zhang, Z.; Prevost, J. H.; Suo, Z. Time-dependent Crack Behavior in an Integrated Structure. *Int. J. Fract.* **2004**, *125* (3−4), 335−348.

(28) Lane, M. W.; Liu, X. H.; Shaw, T. M. Environmental Effects on Cracking and Delamination of Dielectric Films. *IEEE Trans. Device Mater. Reliab.* **2004**, *4* (2), 142−147.

(29) Lane, M. W.; Snodgrass, J. M.; Dauskardt, R. H. Environmental Effects on Interfacial Adhesion. *Microelectron. Reliab.* **2001**, *41* (9−10), 1615−1624.

(30) Li, H.; Tsui, T. Y.; Vlassak, J. J. Water Diffusion and Fracture Behavior in Nanoporous Low-k Dielectric Film Stacks. *J. Appl. Phys.* **2009**, *106* (3), No. 033503.

(31) Lin, Y. B.; Tsui, T. Y.; Vlassak, J. J. Water Diffusion and Fracture in Organosilicate Glass Film Stacks. *Acta Mater.* **2007**, *55* (7), 2455−2464.

(32) Birringer, R. P.; Shaviv, R.; Besser, P. R.; Dauskardt, R. H. Environmentally Assisted Debonding of Copper/barrier Interfaces. *Acta Mater.* **2012**, *60* (5), 2219−2228.

(33) Vellinga, W. P.; De Hosson, J. T. M.; Bouten, P. C. P. Effect of Relative Humidity on Crack Propagation in Barrier Films for Flexible Electronics. *J. Appl. Phys.* **2012**, *112* (8), 083520.

(34) Guan, Q.; Laven, J.; Bouten, P. C. P.; de With, G. Subcritical Crack Growth in SiNx thin-film Barriers Studied by Electro-mechanical Two-point Bending. *J. Appl. Phys.* **2013**, *113* (21), 213512.

(35) Bhatnagar, A.; Hoffman, M. J.; Dauskardt, R. H. Fracture and Subcritical Crack-Growth Behavior of Y-Si-Al-O-N Glasses and Si3N4 Ceramics. *J. Am. Ceram. Soc.* **2000**, *83* (3), 585−596.

(36) Ishihara, S.; McEvily, A. J.; Goshima, T. Effect of Atmospheric Humidity on the Fatigue Crack Propagation Behavior of Short Cracks in Silicon Nitride. *J. Am. Ceram. Soc.* **2000**, *83* (3), 571.

(37) Freund, L. B.; Suresh, S. *Thin Film Materials: Stress, Defect Formation, and Surface Evolution*; Cambridge University Press: Cambridge, U.K., 2003; DOI: 10.1017/CBO9780511754715.

(38) Hutchinson, J. W.; Suo, Z. Mixed Mode Cracking in Layered Materials. *Adv. Appl. Mech.* **1991**, *29*, 63−191.

(39) Favache, A.; Libralesso, L.; Jacques, P. J.; Raskin, J. P.; Bailly, C.; Nysten, B.; Pardoen, T. Fracture Toughness Measurement of Ultra-

DOI: 10.1021/acsami.6b06417
ACS Appl. Mater. Interfaces 2016, 8, 27169−27178

thin Hard Films Deposited on a Polymer Interlayer. *Thin Solid Films* **2014**, *550*, 464−471.
(40) Vlassak, J. J. Channel Cracking in Thin Films on Substrates of Finite Thickness. *Int. J. Fract.* **2003**, *119* (4), 299−323.
(41) Huang, R.; Prevost, J. H.; Huang, Z. Y.; Suo, Z. Channel-cracking of Thin Films with the Extended Finite Element Method. *Eng. Fract. Mech.* **2003**, *70* (18), 2513−2526.
(42) Anderson, T. L. *Fracture Mechanics: Fundamentals and Applications*; CRC Press: Boca Raton, FL, 1995.
(43) Mei, H. X.; Pang, Y. Y.; Huang, R. Influence of Interfacial Delamination on Channel Cracking of Elastic Thin Films. *Int. J. Fract.* **2007**, *148* (4), 331−342.
(44) Thouless, M. D.; Li, Z.; Douville, N. J.; Takayama, S. Periodic Cracking of Films Supported on Compliant Substrates. *J. Mech. Phys. Solids* **2011**, *59* (9), 1927−1937.
(45) Chai, H. Channel Cracking in Inelastic Film/substrate Systems. *Int. J. Solids Struct.* **2011**, *48* (7−8), 1092−1100.
(46) Hu, M. S.; Evans, A. G. The Cracking and Decohesion of Thin-films on Ductile Substrates. *Acta Metall.* **1989**, *37* (3), 917−925.
(47) Walmsley, B.; Liu, Y.; Hu, X. Z.; Bush, M. B.; Dell, J. M.; Faraone, L. Poisson's Ratio of Low-temperature PECVD Silicon Nitride Thin Films. *J. Microelectromech. Syst.* **2007**, *16* (3), 622−627.
(48) *ABAQUS/Standard 6.13, User's Manual*; SIMULIA, Providence, RI, 2010; http://129.97.46.200:2080/v6.13/.
(49) Rice, J. R. A Path Independent Integral and the Approximate Analysis of Strain Concentrations by Notches and Cracks. *J. Appl. Mech.* **1968**, *35* (2), 379−386.
(50) Lee, J. Y.-M.; Sooriakumar, K.; Dange, M. M. The Preparation, Characterization and Application of Plasma-enhanced Chemically Vapour Deposited Silicon Nitride Films Deposited at Low Temperatures. *Thin Solid Films* **1991**, *203* (2), 275−287.
(51) Juang, C.; Chang, J. H.; Hwang, R. Y. Properties of Very Low Temperature Plasma Deposited Silicon Nitride Films. *J. Vac. Sci. Technol., B: Microelectron. Process. Phenom.* **1992**, *10* (3), 1221−1223.
(52) Matoy, K.; Schonherr, H.; Detzel, T.; Schoberl, T.; Pippan, R.; Motz, C.; Dehm, G. A Comparative Micro-cantilever Study of the Mechanical Behavior of Silicon Based Passivation Films. *Thin Solid Films* **2009**, *518* (1), 247−256.
(53) Wiederhorn, S. M.; Freiman, S. W.; Fuller, E. R.; Simmons, C. J. Effects of Water and Other Dielectrics on Crack-growth. *J. Mater. Sci.* **1982**, *17* (12), 3460−3478.
(54) Wiederhorn, S. M.; Fuller, E. R.; Thomson, R. Micro-mechanisms of Crack-Growth in Ceramics and Glasses in Corrosive Environments. *Met. Sci.* **1980**, *14* (8−9), 450−458.
(55) Michalske, T. A.; Bunker, B. C. Slow Fracture Model Based on Strained Silicate Structures. *J. Appl. Phys.* **1984**, *56* (10), 2686.
(56) Michalske, T. A.; Freiman, S. W. A Molecular Mechanism for Stress Corrosion in Vitreous Silica. *J. Am. Ceram. Soc.* **1983**, *66* (4), 284−288.
(57) Laarz, E.; Zhmud, B. V.; Bergstrom, L. Dissolution and Deagglomeration of Silicon Nitride in Aqueous Medium. *J. Am. Ceram. Soc.* **2000**, *83* (10), 2394−2400.
(58) Baumert, E. K.; Pierron, O. N. Fatigue Properties of Atomic-layer-deposited Alumina Ultra-barriers and Their Implications for the Reliability of Flexible Organic Electronics. *Appl. Phys. Lett.* **2012**, *101* (25), 251901−5.
(59) Baumert, E. K.; Pierron, O. N. Erratum:`Fatigue Properties of Atomic-Layer-Deposited Alumina Ultra-Barriers and Their Implications for the Reliability of Flexible Organic Electronics" [Appl. Phys. Lett. 101, 251901 (2012)]. *Appl. Phys. Lett.* **2013**, *102* (5), 059902.
(60) Baumert, E. K.; Pierron, O. N. Interfacial Cyclic Fatigue of Atomic-Layer-Deposited Alumina Coatings on Silicon Thin Films. *ACS Appl. Mater. Interfaces* **2013**, *5* (13), 6216−6224.
(61) Zhang, Y. D.; Yang, R. G.; George, S. M.; Lee, Y. C. In-situ Inspection of Cracking In Atomic-layer-deposited Barrier Films on Surface and in Buried Structures. *Thin Solid Films* **2011**, *520* (1), 251−257.
(62) Sénémaud, C.; Driss-Khodja, M.; Gheorghiu, A.; Harel, S.; Dufour, G.; Roulet, H. Electronic Structure of Silicon Nitride Studied by Both Soft X-Ray Spectroscopy and Photoelectron Spectroscopy. *J. Appl. Phys.* **1993**, *74* (8), 5042−5046.
(63) Ingo, G. M.; Zacchetti, N.; della Sala, D.; Coluzza, C. X-ray Photoelectron Spectroscopy Investigation on the Chemical Structure of Amorphous Silicon Nitride (a-SiNx). *J. Vac. Sci. Technol., A* **1989**, *7* (5), 3048−3055.
(64) Finster, J. SiO2 in 6:3 (Stishovite) and 4:2 Co-ordination—Characterization by Core Level Spectroscopy (XPS/XAES). *Surf. Interface Anal.* **1988**, *12* (5), 309−314.
(65) Taylor, J. A.; Lancaster, G. M.; Ignatiev, A.; Rabalais, J. W. Interactions of Ion Beams with Surfaces. Reactions of Nitrogen with Silicon and Its Oxides. *J. Chem. Phys.* **1978**, *68* (4), 1776−1784.

DOI: 10.1021/acsami.6b06417
ACS Appl. Mater. Interfaces 2016, 8, 27169−27178